

## Contact Angle and Condensation of a CO<sub>2</sub> Droplet on a Solid Surface

Jiayang Wu,<sup>1,2,\*</sup> Åsmund Ervik,<sup>3</sup> Ingrid Snustad,<sup>1</sup> Senbo Xiao,<sup>1</sup> Amy Brunsvold,<sup>3</sup> Jianying He<sup>1</sup> and Zhiliang Zhang<sup>1,\*</sup>

<sup>1</sup>NTNU Nanomechanical Lab, Norwegian University of Science and Technology (NTNU), Trondheim 7491, Norway

<sup>2</sup>Department of Physics, Research Institute for Biomimetics and Soft Matter, Jiujiang Research Institute and Fujian Provincial Key Laboratory for Soft Functional Materials Research, Xiamen University, Xiamen 361005, PR China

<sup>3</sup>SINTEF Energy Research, P. O. Box 4761 Sluppen, Trondheim 7465, Norway

**Abstract:** Anthropogenic release of carbon dioxide (CO<sub>2</sub>) is a major contribution to manmade increase in global warming. Carbon Capture and Storage (CCS) is a necessary technology for lowering CO<sub>2</sub> emissions to an acceptable level that limits global warming to below 2 degrees. Liquefaction of CO<sub>2</sub> is a key process both in capture technologies and in conditioning before ship transport. The efficiency of this process can be remarkably enhanced by promoting dropwise CO<sub>2</sub> condensation on cooling surfaces, yet this remains largely unexplored. Here, using molecular dynamics (MD) simulations, we report for the first time the contact angle and condensation behaviour of CO<sub>2</sub> droplets on a smooth solid surface. The contact angle of the condensed CO<sub>2</sub> droplet is greatly dependent on the CO<sub>2</sub>-solid characteristic interaction energy, but this does not hold true for the sum of condensed molecules. In contrast, the sum of condensed molecules for the filmwise condensation regime increases monotonically at first, but then remains constant as the CO<sub>2</sub>-solid interaction energy approaches to a critical value. It is also revealed that droplet condensation on a cooling surface shows three distinct stages that are primarily characterized by heterogeneous cluster nucleation, diffusion-coalescence, and Ostwald ripening-coalescence mechanisms. As the area of the solid surface is increased by diffusion-induced coalescence of clusters at the first stage, cluster nucleation proceeds but ceases in the last stage at which the sum of condensed molecules are not accumulated. Analysis of the Ostwald ripening kinetics of a CO<sub>2</sub> droplet reveals a constant growth rate of around 11 CO<sub>2</sub> molecules/ns of the droplet.

---

\*Corresponding emails: [jiayang@xmu.edu.cn](mailto:jiayang@xmu.edu.cn), [zhiliang.zhang@ntnu.no](mailto:zhiliang.zhang@ntnu.no)

## 1. Introduction

Carbon dioxide (CO<sub>2</sub>) is one of the dominant gases contributing to the earth's greenhouse effect. Anthropogenic release of CO<sub>2</sub> from fossile sources contributes to an increased global warming, with potentially catastrophic consequences. Substantial reduction of CO<sub>2</sub> emissions from industrial processes such as power generation, steel and cement production, etc. by combustion of fossil fuels is necessary to restrain and reverse the global warming process. Beyond those negative impacts, however, CO<sub>2</sub> also finds versatile important applications, such as in fire extinguishers, as a safe refrigerant and coolant, used in the brewing of soft drinks, beers and other alcoholic drinks, for softening water to avoid corrosion, producing potable water, enhancing oil recovery (EOR), sand blasting, hardening of metal castings, and so forth<sup>1-7</sup>. Utilization of CO<sub>2</sub> as a byproduct not only provides significant economic benefits but can also in some cases mitigate global warming and climate change concerns. There is, thus, a rapid growth in both academic research activities and industrial research and development (R&D) programmes worldwide to explore solutions for controlling CO<sub>2</sub> emissions.

Carbon Capture and Storage (CCS) is considered as one of the most effective CO<sub>2</sub> emission abatement strategies to combat climate change migration<sup>8-10</sup>. Generally, there are three emerging pathways for CO<sub>2</sub> capture, including pre-combustion, post-combustion, and oxy-fuel processes<sup>6-9, 11-12</sup>. Among them, the post-combustion is well understood, has lower capital expenditure (CAPEX) and is favored for CO<sub>2</sub> capture projects in the short-term. To date, a variety of technologies has been emerged for post-combustion CO<sub>2</sub> capture, including adsorption, physical absorption, chemical absorption, cryogenics separation and membranes<sup>13-16</sup>. While these technologies are rapidly being matured for post-combustion power plants, the main drawback is the high-energy penalties that must be paid. Moreover, although the aqueous organic amine-based method is relatively mature for post-combustion CO<sub>2</sub> capture, this technology shows several drawbacks including toxicity, degradation, and evaporation of the solvent<sup>10</sup>. Recently, CO<sub>2</sub> capture by mineralization (CO<sub>2</sub> molecules react with

1  
2  
3 the cationic metal atoms in expandable clays to form carbonate minerals) was proposed and  
4 investigated<sup>17-18</sup>.  
5  
6

7  
8 Inspired by water or fog harvest by droplet condensation on hydrophobic-functionalized or patterned  
9 solid surfaces<sup>19-22</sup>, a relatively novel CO<sub>2</sub> capture technology by dropwise CO<sub>2</sub> condensation on  
10 cooling surfaces has been recently envisaged<sup>23</sup>. Gaseous CO<sub>2</sub> is expected to condense as liquid  
11 droplets onto functionalized surfaces of heat exchangers that are cooled. An advantage of this  
12 conditioning process may enable a potentially improved low temperature capture technique and no  
13 chemical absorbents are needed. To date, researches on CO<sub>2</sub> condensation on solid surfaces are  
14 extremely rare<sup>23-24</sup>, although there have been investigations on cooling of CO<sub>2</sub> that mainly  
15 concentrated on supercritical gas cooling and wettability of water on solid surfaces upon CO<sub>2</sub> pressure  
16 <sup>25-33</sup>. Understanding the fundamental wetting and condensation behaviours of CO<sub>2</sub> on a cooling surface  
17 is a necessary starting point for CO<sub>2</sub> capture by the technology. Molecular dynamics (MD) simulation  
18 has become an indispensable tool for investigating details of water condensation, wettability and  
19 nucleation on functionalized and patterned solid surfaces<sup>34-42</sup>. Since experimental measurements of  
20 the contact angle of liquid CO<sub>2</sub> on functionalized surfaces currently under development are yet to be  
21 performed, the interaction energy between the CO<sub>2</sub> and substrate is considered as a free parameter in  
22 this work, spanning the range of contact angles. The functionalized surfaces are likely to be made from  
23 (or contain a high percentage of) copper, due to the excellent heat transfer properties of this material,  
24 and thus we consider a copper substrate. In this work, we present, for the first time, the contact angle  
25 and condensation of CO<sub>2</sub> on cooling solid surface by large-scale MD simulations.  
26  
27  
28  
29  
30  
31  
32  
33  
34  
35  
36  
37  
38  
39  
40  
41  
42  
43  
44  
45  
46  
47  
48  
49

## 50 **2. Methods**

51  
52  
53 All the MD simulations are implemented by the LAMMPS MD simulation package. A many-body  
54 interatomic potential of embedded-atom method (EAM) derived by Mishin et al.<sup>43</sup> is adopted to model  
55  
56  
57  
58  
59  
60

the interatomic interactions in a face-cubic-center (fcc) copper (Cu) surface with a (1 0 0) surface. In this EAM forcefield<sup>44</sup>, the total potential energy of an elemental system is given by

$$E = \frac{1}{2} \sum_{ij} U(r_{ij}) + \sum_{ij} F(\bar{\rho}_i) \quad (1)$$

where

$$\bar{\rho}_i = \sum_{j \neq i} \rho(r_{ij}) \quad (2)$$

Here  $U(r_{ij})$  is a pair-wise potential as a function of distance ( $r_{ij}$ ) between atom  $i$  and atom  $j$ .  $F(\bar{\rho}_i)$  is the embedding energy required to place an atom into the host electron density  $\bar{\rho}_i$  that is the sum of the contributions  $\rho(r_{ij})$  from all the other atoms in the system.

The pairwise potential function is expressed as

$$U(r) = [E_1 M(r, r_0^{(1)}, \alpha_1) + E_2 M(r, r_0^{(2)}, \alpha_2) + \delta] \times \psi\left(\frac{r-r_c}{h}\right) - \sum_{n=1}^3 H(r_s^{(n)} - r) S_n(r_s^{(n)} - r)^4 \quad (3)$$

where

$$M(r, r_0, \alpha) = \exp[-2\alpha(r-r_0)] - 2\exp[-\alpha(r-r_0)] \quad (4)$$

$$\psi(x) = \begin{cases} 0, & x \geq 0 \\ \frac{x^4}{x^4+1}, & x < 0 \end{cases} \quad (5)$$

are a Morse function and a cutoff function, respectively. The embedding function is written as

$$F(\bar{\rho}) = \begin{cases} F^{(0)} + \frac{1}{2}F^{(2)}(\bar{\rho}-1)^2 + \sum_{n=1}^4 q_n(\bar{\rho}-1)^{n+2}, & \bar{\rho} \leq 1 \\ \frac{F^{(0)} + \frac{1}{2}F^{(2)}(\bar{\rho}-1)^2 + q_1(\bar{\rho}-1)^3 + Q_1(\bar{\rho}-1)^4}{1 + Q_2(\bar{\rho}-1)^3}, & \bar{\rho} > 1 \end{cases} \quad (6)$$

The potential is capable to reproduce various properties of Cu, such as lattice properties, elastic constants, thermal expansion, point and extended defects, and epitaxial growth of Cu films on (0 0 1)-oriented *fcc* or body-centered-cubic (bcc) substrates<sup>43</sup>. For the CO<sub>2</sub> modelling, the efficient and accurate coarse-grained (CG) forcefield of SAFT- $\gamma$  Mie potential is used for the intermolecular interactions of CO<sub>2</sub>. The functional form of CG SAFT- $\gamma$  Mie potential is expressed as<sup>45-46</sup>

$$\phi^{\text{Mie}}(r) = \varepsilon C(\lambda_a, \lambda_r) \left[ \left( \frac{\sigma}{r} \right)^{\lambda_r} - \left( \frac{\sigma}{r} \right)^{\lambda_a} \right] \quad (7)$$

where

$$C(\lambda_a, \lambda_r) = \left( \frac{\lambda_r}{\lambda_r - \lambda_a} \right) \left( \frac{\lambda_r}{\lambda_a} \right)^\beta \quad \text{with } \beta = \left( \frac{\lambda_a}{\lambda_r - \lambda_a} \right) \quad (8)$$

where  $r$ ,  $\varepsilon$  and  $\sigma$  are the intermolecular distance, the depth of the potential well and the diameter of the CO<sub>2</sub> CG bead, respectively.  $\lambda_r$  and  $\lambda_a$  are the repulsive and attractive exponents of the molecular bead-bead interactions which characterize the pair energy. The SAFT- $\gamma$  Mie forcefield parameters  $\sigma$ ,  $\lambda_r$  and  $\lambda_a$  are 3.741 Å, 23.0 and 6.66 for CG CO<sub>2</sub> bead, respectively<sup>45</sup>. The diameter of the CO<sub>2</sub> CG bead is similar to the lattice constant of *fcc* Cu. The Mie potential is also adopted to describe the interaction between CO<sub>2</sub> molecules and Cu-like solid surface. The energy interaction parameter  $\varepsilon_{\text{CO}_2\text{-Cu}}$  varies from 0.001-0.1 eV to fully cover the surface properties of a solid-surface from CO<sub>2</sub>-phobic to

CO<sub>2</sub>-philic. The main purpose of using Cu substrate is to provide a physical solid state for CO<sub>2</sub> to adsorb. By varying the energy interaction parameter between CO<sub>2</sub> and the substrate, the MD simulations can qualitatively predict CO<sub>2</sub> adsorbing dynamics and possibly equilibrium contact angles on the substrates with different surface energies. For the sake of simplicity, the internal interactions between the substrate atoms, namely Cu atoms, were kept the same in all the simulations for maintaining the integrity of the substrate, and to provide constant surface structure. In reality, it is only possible to use other atom types, for instances, Fe, Al or Au, to provide different energy interaction parameter  $\epsilon$  between CO<sub>2</sub> and the flat substrate. Yet, different atoms types will result in different surface lattice structure and size, which are also important factors for CO<sub>2</sub> condensation. Such complexity is beyond the scope of the current study. The cutoff distance of 15 Å is utilized for the CG *Mie* potential interactions. The velocity-Verlet method is employed to integrate the equation of atomic motions with a timestep of 10 fs in all cases.

### 3. Results and discussion

To validate the implemented SAFT- $\gamma$  Mie model of CO<sub>2</sub>, the temperature-density vapor-liquid equilibria (VLE) curve is studied. A slab consisting of 18450 CO<sub>2</sub> molecules is initially placed in the center of an otherwise empty simulation box with dimensions of 92 Å × 92 Å × 500 Å. The system is then fully equilibrated in an NVT ensemble with sufficient simulation time of 10 ns to achieve a stable liquid film in equilibrium with its vapor phase, as shown in Figure 1a. Figure 1b presents the density profiles obtained by averaging over the last 20000 timesteps in the vapor-liquid system at temperatures ranging from 220 K - 290 K. Each bin is set in 2.5 Å for calculating the density of CO<sub>2</sub>. Similar to previous studies, the density profiles of local vapor-liquid interface can be well-fitted by both tangent hyperbolic and error functions<sup>47-48</sup> that are respectively written as

$$\rho(z) = \frac{1}{2}(\rho_l + \rho_v) - \frac{1}{2}(\rho_l - \rho_v) \tanh\left[\frac{2}{d}(z-1)\right] \quad (9)$$

and

$$\rho(z) = \frac{1}{2}(\rho_l + \rho_v) - \frac{1}{2}(\rho_l - \rho_v) \operatorname{erf} \left[ \frac{\sqrt{\pi}}{d} (z - l) \right] \quad (10)$$

where  $\rho_l$  and  $\rho_v$  are the densities of liquid and vapor in equilibrium, respectively.  $l$  and  $d$  are the middle-position of the equilibrium vapor-liquid interface and the thickness parameter, respectively. As expected, the liquid density and the number of molecules in the liquid CO<sub>2</sub> declines with increasing temperature, while the vapor density increases. This suggests that, upon cooling, vapor of CO<sub>2</sub> tends to condense on the liquid slab to balance the vapor-liquid equilibrium. Figure 1c compares the predicted vapor-liquid coexistence densities of CO<sub>2</sub> by MD simulation with those calculated using the Span-Wagner (SW) equation of state (EoS) with the methodology given in Ref. 46. There is a good agreement between the MD simulation and SW EoS for the temperature-density distribution of CO<sub>2</sub> phase diagram<sup>49-50</sup>. This confirms that the SAFT- $\gamma$  CG Mie model of CO<sub>2</sub> is correctly implemented and this model is able to predict the bulk thermodynamic properties<sup>45</sup>. Other works have verified that the model also yields accurate predictions the vapor-liquid interfacial behaviour for the CO<sub>2</sub> molecules<sup>51-52</sup>.

With accurate models for the CO<sub>2</sub> and the surface, we proceed to study the evolution of a CO<sub>2</sub> nanodroplet on a Cu-like smooth solid surface. An initial CO<sub>2</sub> cubic box containing 43537 CO<sub>2</sub> CG beads is placed on the Cu-like flat surface with 2D planar dimensions of 400 Å × 400 Å. Within a sufficient equilibration simulation time of 50 ns at 223.15 K, the initially generated CO<sub>2</sub> box evolves to a mixture of vapor-liquid droplet or a mixture of vapor-liquid film, depending on surface wettability. In the simulations, there is no integration of motion for the Cu-like solid surface. The coordinates of each beads are collected in every 100 ps for monitoring the development of the CO<sub>2</sub> droplet, and the density contours of CO<sub>2</sub> are obtained by taking samples of the dynamic droplet at every 10000 timesteps for the last simulation of 1 ns. Figure 2 shows the calculated 2D density contours of the CO<sub>2</sub> droplet on Cu-like surface ( $z = 10$  Å) with different wettability. Apparently, liquid-state CO<sub>2</sub> molecules are more strongly attracted by a CO<sub>2</sub>-philic Cu-like surface than by a CO<sub>2</sub>-phobic Cu-like surface as

1  
2  
3 the solid-CO<sub>2</sub> characteristic energy is increased. Here, a symbol  $\varepsilon_{\text{CO}_2\text{-Cu}}$  is used to denote the parameter  
4  
5 of interaction between copper and CO<sub>2</sub>. The range of  $\varepsilon_{\text{CO}_2\text{-Cu}}$  from 0.001 to 0.015 eV is able to cover  
6  
7 the surface wettability perfectly, changing from CO<sub>2</sub>-phobic to CO<sub>2</sub>-philic. As  $\varepsilon_{\text{CO}_2\text{-Cu}}$  is 0.001 eV, a  
8  
9 stable spherical CO<sub>2</sub>-droplet is suspended in the vapor without contacting the Cu-like surface,  
10  
11 indicating a perfect CO<sub>2</sub>-phobicity (Figure 2a). When the  $\varepsilon_{\text{CO}_2\text{-Cu}}$  varies from 0.003 to 0.012 eV, very  
12  
13 clearly the shape of a CO<sub>2</sub> droplet on the Cu-like surface is identified (Figure 2b-g). As  $\varepsilon_{\text{CO}_2\text{-Cu}}$  becomes  
14  
15 larger ( $\geq 0.015$  eV), the Cu-like surface shows a perfect CO<sub>2</sub>-philicity (Figure 2h). An inhomogeneity  
16  
17 in the density of CO<sub>2</sub> in the droplet is identified, especially near the droplet and the Cu-like surfaces.  
18  
19 Notably, the boundaries between liquid and gas phases of CO<sub>2</sub> are distinguished by the green-  
20  
21 highlighted region in the relative density contour plots. In the vicinity of the Cu-like surface with  
22  
23  $\varepsilon_{\text{CO}_2\text{-Cu}}$  ranging from 0.008 to 0.012 eV, formation of a four-layer CO<sub>2</sub> sheet with thickness of around  
24  
25 10.6 Å, separating the Cu-like solid surface and the rest of the droplet, is observed (Figure 2d-g). The  
26  
27 thickness of each layer (2.65 Å) implies that the layers are monomolecular. The density of liquid CO<sub>2</sub>  
28  
29 near the Cu-like surface declines as the layer is moving away from the Cu-like surface. For the Cu-  
30  
31 like surface with higher CO<sub>2</sub>-phobicity, the number of CO<sub>2</sub> layers near the Cu-like surface decreases  
32  
33 (Figure 2b and c). With respect to the Cu-like surface with a perfect CO<sub>2</sub>-philicity ( $\varepsilon_{\text{CO}_2\text{-Cu}} = 0.015$  eV),  
34  
35 an apparent CO<sub>2</sub> tri-layer is formed and the layer nearest to the Cu-like surface shows higher density  
36  
37 than the other layers.  
38  
39  
40  
41  
42  
43  
44  
45  
46  
47

48 Figure 3a presents a representative equilibrium snapshot of a CO<sub>2</sub> droplet on the Cu-like surface  
49  
50 ( $\varepsilon_{\text{CO}_2\text{-Cu}} = 0.008$  eV). Unlike for a water droplet in air on a solid surface, the vapor and liquid here  
51  
52 consist of the same fluid molecules, so the liquid droplet (blue) and vapor (yellow) of CO<sub>2</sub> coexist in  
53  
54 the simulation system. The contact angle  $\theta_c$  of a CO<sub>2</sub> droplet on the Cu-like surface is defined by the  
55  
56 tangent at the contact line, as illustrated in Figure 2d. Figure 3b plots the calculated contact angle  $\theta_c$   
57  
58  
59  
60



1  
2  
3 of a CO<sub>2</sub> droplet as a function of the CO<sub>2</sub>-surface interaction  $\varepsilon_{\text{CO}_2\text{-Cu}}$ . As expected, the contact angle is  
4  
5 sensitive to the interaction energy  $\varepsilon_{\text{CO}_2\text{-Cu}}$  between CO<sub>2</sub> molecules and the attractive surface. The  
6  
7 contact angle monotonically decreases from 180° to 0° with  $\varepsilon_{\text{CO}_2\text{-Cu}}$  increasing from 0.001-0.015 eV.  
8  
9 Large  $\varepsilon_{\text{CO}_2\text{-Cu}} > 0.015$  eV leads to complete spreading of the CO<sub>2</sub> droplet and wetting of the solid  
10  
11 surface. Particularly, an energy interaction parameter  $\varepsilon_{\text{CO}_2\text{-Cu}}$  of 0.009 eV (the liquid-solid tension of  
12  
13 around 10 mN/m) yields a contact angle of approximately 90° of a CO<sub>2</sub> droplet, which is the critical  
14  
15 point for transition from CO<sub>2</sub>-phobic to CO<sub>2</sub>-philic. Figure 3c and 3d plot the number of liquid CO<sub>2</sub>  
16  
17 molecules and the density of CO<sub>2</sub> vapor as a function of simulation time for different Cu-like surface  
18  
19 wettability. For all our studied systems with different wettability of surfaces, two stages in the curves  
20  
21 can be roughly identified. The first stage is characterized by a monotonic reduction in number of liquid  
22  
23 molecules or an increase in density of the CO<sub>2</sub> vapor. This quantitatively illustrates the vaporization  
24  
25 process of liquid CO<sub>2</sub>. The initial vaporization rate is closely related to the energy interaction parameter  
26  
27  $\varepsilon_{\text{CO}_2\text{-Cu}}$ . For an energy interaction parameter  $\varepsilon_{\text{CO}_2\text{-Cu}}$  between 0.001 and 0.02 eV, a small difference in  
28  
29 the initial vaporization rate is observed. When it is  $> 0.02$  eV, however, the initial vaporization rate  
30  
31 shows a decreasing trend. Moreover, the vaporization rate declines with the simulation time. The  
32  
33 second stage corresponds to the long plateau in the curves. This indicates the vapor-liquid equilibrium  
34  
35 for CO<sub>2</sub> contacting a Cu-like surface. Figure 3e and 3f plot the equilibrated number of liquid CO<sub>2</sub>  
36  
37 molecules and the CO<sub>2</sub> vapor density, respectively, as function of the energy interaction parameter  
38  
39  $\varepsilon_{\text{CO}_2\text{-Cu}}$ , respectively. Intriguingly, for the energy interaction parameter  $\varepsilon_{\text{CO}_2\text{-Cu}}$  yielding a non-zero  
40  
41 contact angle of a droplet, there is a negligible difference in the total number of CO<sub>2</sub> molecules in  
42  
43 liquid-state. As the solid surface becomes more CO<sub>2</sub>-philic, however, the number of liquid CO<sub>2</sub>  
44  
45 molecules increases pronouncedly. This is because more CO<sub>2</sub> molecules are attracted by the Cu-like  
46  
47 surface with strong attractive interaction. Notably, the number of liquid CO<sub>2</sub> molecules remains  
48  
49 constant as the energy interaction parameter  $\varepsilon_{\text{CO}_2\text{-Cu}}$  approaches to 0.05 eV. This can be explained by  
50  
51  
52  
53  
54  
55  
56  
57  
58  
59  
60

1  
2  
3 the fact that the number of CO<sub>2</sub> layers adsorbed on the solid surface is limited by applying a cutoff of  
4 non-bonded interaction. For the variation of density of CO<sub>2</sub> vapor with  $\epsilon_{\text{CO}_2\text{-Cu}}$ , an opposite tendency  
5  
6  
7  
8 can be seen in Figure 3f.  
9

10  
11 Condensation of CO<sub>2</sub> on the Cu-like surface for  $\epsilon_{\text{CO}_2\text{-Cu}} = 0.008$  eV is further studied. Initially, the  
12 stable droplet is vaporized at 273.15 K for a sufficient time of 50 ns under NVT (constant number of  
13 particles, constant volume, and constant temperature) ensemble. For the condensation simulation, a  
14 novel combination of MD simulation setups is adopted. The outmost layer of the Cu-like atoms is  
15 fixed to prevent the deformation of the solid surface. The inside two layers of the Cu-like atoms are  
16 simulated at 223.15 K under NVT ensemble as cooling source. MD simulations of the top outside three  
17 layers of Cu atoms and the CO<sub>2</sub> molecules are performed under NVE (constant number of particles,  
18 constant volume, and constant energy) ensemble for exchanging energy between CO<sub>2</sub> and the cooling  
19 layers. A long-enough simulation time of around 125 ns is assigned for mimicking the condensation  
20 process. The kinetics of the CO<sub>2</sub> condensation on the Cu-like surface is characterized by the analysis  
21 of the droplet size (molecular number). Figure 4a shows the variations in the number of liquid CO<sub>2</sub>  
22 molecules and the density of the vapor phase within the whole simulation time span. During  
23 vaporization (grey region), the droplet is fully vaporized at about 7 ns and the vaporization of the  
24 droplet becomes less pronounced as indicated by the reduction in  $\frac{d\rho}{dt}$ . From 7-50 ns, the system is  
25 mainly composed of CO<sub>2</sub> vapor contacting the Cu-like surface. In the curve of CO<sub>2</sub> condensation from  
26 50-75 ns, the number of liquid CO<sub>2</sub> molecules rapidly increases to a constant in response to cooling  
27 (red curve of Figure 4a). Meanwhile, the density of CO<sub>2</sub> vapor decreases to a constant as a result of  
28 the law of conservation of mass. Both events quantitatively explain the CO<sub>2</sub> condensation on the Cu-  
29 like surface. Figure 4b plots the sum interaction forces between CO<sub>2</sub> molecules and the Cu-like surface  
30 in the three orthogonal directions. In the planar directions of the surface, the sum interaction forces  
31 oscillate around zero in both the vaporization and the condensation processes. In contrast, the average  
32  
33  
34  
35  
36  
37  
38  
39  
40  
41  
42  
43  
44  
45  
46  
47  
48  
49  
50  
51  
52  
53  
54  
55  
56  
57  
58  
59  
60

1  
2  
3 total interaction force in the vertical ( $z$ ) direction shows a similar tendency to the number of liquid CO<sub>2</sub>  
4 molecules. At complete vaporization, an average interaction force of around  $-2.8 \text{ eV/\AA}$  is yielded. At  
5  
6  
7  
8 late phases of condensation, however, the system shows a mean interaction force of about  $-1.25 \text{ eV/\AA}$ .  
9  
10 Such a difference is mainly attributed to the mean distance of the center of mass position between CO<sub>2</sub>  
11 and surface in the vertical direction.  
12  
13

14  
15 To reveal the kinetic mechanism of cooling-induced CO<sub>2</sub> condensation, a series of top-viewed  
16 snapshots, in which gas molecules are removed, are captured at different condensation times as shown  
17  
18 in Figure 4c. At 40 ns, no droplet is identified, indicating that the original droplet is completely  
19 vaporized. The condensation process of a CO<sub>2</sub> droplet on a Cu-like cooling surface is roughly divided  
20 into three stages. The first stage corresponds to the nucleation of CO<sub>2</sub> clusters as illustrated by the  
21 snapshot captured at 50.5 ns. It is observed that a large number of CO<sub>2</sub> clusters heterogeneously  
22 nucleate on the Cu-like cooling surface at the same time. This stage is a very rapid process. The second  
23 stage of the condensation process is primarily characterized by formation of droplets via coalescence  
24 and growth of CO<sub>2</sub> clusters as seen in snapshots captured from 52-66.3 ns. The nucleated CO<sub>2</sub> clusters  
25 dynamically form droplets by diffusion of CO<sub>2</sub> vapor molecules from the surroundings. CO<sub>2</sub> droplets  
26 are also formed by coalescence of nearby CO<sub>2</sub> clusters due to their strong non-bonded attractions. The  
27 droplet growth by coalescence does not increase the condensed mass of CO<sub>2</sub> on the Cu-like surface, in  
28 contrast to droplet growth by diffusion. Moreover, because the contacting area of the solid-surface is  
29 increased by the coalescence of neighboring nucleated clusters and droplets, fresh clusters or droplets  
30 grow by nucleation and diffusion. The final stage of the process is uniquely characterized by Ostwald  
31 ripening-coalescence mechanisms of CO<sub>2</sub> droplets. This stage lasts from around 66.7- 175 ns. The  
32 long-plateau characteristic in the curves of Figure 4a indicates that there is no growth of droplet by  
33 diffusion of CO<sub>2</sub> molecules from the vapor. As a result of the Ostwald ripening and coalescence  
34 behaviour, a single stable droplet finally condenses on the cooling Cu-like surface within  
35  
36  
37  
38  
39  
40  
41  
42  
43  
44  
45  
46  
47  
48  
49  
50  
51  
52  
53  
54  
55  
56  
57  
58  
59  
60

1  
2  
3 approximately 174 ns. During the whole condensation process, the condensed droplets show higher  
4 potential energy at the surface than in the interior due to the surface effect.  
5  
6  
7

8 To gain more insights into the Ostwald ripening behaviour during the CO<sub>2</sub> condensation process,  
9 the two large condensed droplets on the Cu-like surface at the final stage are further characterized.  
10 Figure 5a monitors the numbers of CO<sub>2</sub> molecules ( $N_1$  and  $N_2$ ) in droplet #1 and droplet #2, as well as  
11 the sum number of liquid CO<sub>2</sub> molecules ( $N$ ). The two condensed droplets show an opposite trend in  
12 the sum of the molecules. The sum of the molecules  $N_1$  in droplet #1 almost increases linearly from  
13 around 14000 to 20000 with increasing condensation time, whereas in case of droplet #2 it decreases  
14 linearly from about 9000 to 3500 within the same time. By linearly fitting the curves, the corresponding  
15 growth rate and reduction rate of the two droplets are determined to be around 54 and 53 molecules/ns,  
16 respectively. Although there exists great variation in the sum of the CO<sub>2</sub> molecules in both droplets,  
17 the total number of liquid molecules remains constant. To quantitatively explain the molecular  
18 exchanges between the two-condensed droplets, the CO<sub>2</sub> molecules in droplet #1 at 66.5 ns are  
19 specifically marked and traced. Figure 5b shows the sums of marked CO<sub>2</sub> molecules in both droplets  
20 ( $n_1$  and  $n_2$ ) as a function of condensation time. The sum of marked molecules  $n_1$  ( $n_2$ ) monotonically  
21 decreases (increases) with time. Interestingly, the variation rates of  $n_1$  and  $n_2$ , however, are  
22 condensation time dependent. A steep drop (rise) in  $n_1$  ( $n_2$ ) from around 9000 to 2000 (0 to 3000)  
23 within approximately 6.0 ns is identified. Soon afterwards, a nearly linear increase (decrease) in  $n_1$  ( $n_2$ )  
24 is found. A constant variation rate of around 11 molecules/ns for both  $n_1$  and  $n_2$  is determined by fitting  
25 the linear part of the curves in the late phase, which is around 3-fold smaller than the growth rate of  
26 droplet #1 and the decay rate of droplet #2, respectively. Moreover, to further reveal the Ostwald  
27 ripening-coalescence mechanisms for CO<sub>2</sub> condensation on the Cu-like surface, a set of snapshots, in  
28 which the two condensed droplets are purple- and yellow-colored, captured at different times (from  
29 66.5 to 168.5 ns) are shown in Figure 5c. Besides the size change of droplets by molecular exchange  
30 and diffusion, it is observed that both droplets migrate on the Cu-like smooth surface when one droplet  
31  
32  
33  
34  
35  
36  
37  
38  
39  
40  
41  
42  
43  
44  
45  
46  
47  
48  
49  
50  
51  
52  
53  
54  
55  
56  
57  
58  
59  
60

1  
2  
3 is far from the other. As the distance between condensed droplets becomes critical, droplets rapidly  
4  
5 coalesce due to their attractive interaction forces. As a consequence, a single droplet with constant size  
6  
7 finally condensed on the Cu-like surface. This suggests that the distance between droplets is a critical  
8  
9 parameter to determine the Ostwald ripening and coalescence mechanisms during the CO<sub>2</sub>  
10  
11 condensation. It is also found that the marked CO<sub>2</sub> molecules are homogeneously distributed in the  
12  
13 droplets during the condensation process. This indicates that the molecules in the droplets are able to  
14  
15 rapidly diffuse from the interior to the surface and also to the zone of CO<sub>2</sub> vapor.  
16  
17  
18  
19

#### 20 4. Conclusions

21  
22  
23 In summary, contact angle and dropwise condensation of water on different solid surfaces have been  
24  
25 subjected to extensive research. By designing the solid surface structures, dropwise condensation of  
26  
27 water vapor can be achieved for water collection. However, as far as we know, literature on a solid  
28  
29 surface for dropwise CO<sub>2</sub> condensation is virtually non-existing. In this study, classic MD simulations  
30  
31 with accurate forcefields are performed to investigate the condensation and the contact angle of a CO<sub>2</sub>  
32  
33 droplet on a Cu-like solid surface for CO<sub>2</sub> capture. Depending on the wettability of the Cu-like surface,  
34  
35 either dropwise or filmwise condensation of CO<sub>2</sub> is achieved. For droplet condensation on the  
36  
37 macroscale, there exists a transition from CO<sub>2</sub>-phobic to CO<sub>2</sub>-philic at a critical energy interaction  
38  
39 parameter of  $\varepsilon_{\text{CO}_2\text{-Cu}} = 0.009$  eV (corresponding to a liquid-solid tension of approximately 10 mN/m);  
40  
41 however, the sum of condensed CO<sub>2</sub> molecules on a solid surface is insensitive to the energy  
42  
43 interaction parameter  $\varepsilon_{\text{CO}_2\text{-Cu}}$ . For filmwise condensation, the sum of condensed CO<sub>2</sub> molecules  
44  
45 significantly increases as the energy interaction parameter  $\varepsilon_{\text{CO}_2\text{-Cu}}$  increases from 0.012 to 0.050 eV,  
46  
47 but remains constant with further increase of  $\varepsilon_{\text{CO}_2\text{-Cu}}$ . Condensation of a CO<sub>2</sub> droplet on a Cu-like  
48  
49 surface exhibits three distinct stages. In the first stage, heterogeneous nucleation of clusters is dominant  
50  
51 and the nucleation rate is fairly fast. The second stage of condensation is primarily characterized by  
52  
53 cluster growth to droplets via diffusion-coalescence mechanisms. The large-scale coalescence of  
54  
55  
56  
57  
58  
59  
60

1  
2  
3 clusters as droplets arises from cluster diffusion and strong attraction between short-distanced  
4  
5 neighboring clusters. Finally, a combination of Ostwald ripening in which one droplet continues to  
6  
7 grow as function of time ( $\sim t$ ) while the other simultaneously decreases as function of time ( $\sim t$ ), and  
8  
9 the coalescence mainly dominates in the last stage of the condensation process. Considerable  
10  
11 molecular exchange between droplets occurs via fast diffusion. These results provide guidance for the  
12  
13 design of functionalized surfaces to promote dropwise condensation of CO<sub>2</sub>, as well as insight into the  
14  
15 condensation behaviour that will occur on such surfaces  
16  
17  
18  
19

## 20 **Acknowledgments**

21  
22 This work is financially supported by the Research Council of Norway (RCN) through the CLIMIT  
23  
24 program project NanoDrop (Grant No. 254813), the National Natural Science Foundation of China  
25  
26 (Grant Nos. 11772278 and 11502221), the Fundamental Research Funds for the Central Universities  
27  
28 (Xiamen University: Grant Nos. 20720180014, 20720180018 and 20720160088), Fujian Provincial  
29  
30 Department of Science & Technology (2017J05028), Doctoral Fund of the Ministry of Education  
31  
32 (20130121110018), “111” Project (B16029) and the 1000 Talents Program from Xiamen University.  
33  
34 The computational resources are provided by the Norwegian Metacenter for Computational Science  
35  
36 (NOTUR NN9110K and NN9391K).  
37  
38  
39  
40

## 41 **References**

- 42  
43 1. Meylan, F. D.; Moreau, V.; Erkman, S., CO<sub>2</sub> Utilization in the Perspective of Industrial  
44  
45 Ecology, an Overview. *Journal of CO<sub>2</sub> Utilization* **2015**, *12*, 101-108.
- 46  
47 2. Song, C., Global Challenges and Strategies for Control, Conversion and Utilization of CO<sub>2</sub> for  
48  
49 Sustainable Development Involving Energy, Catalysis, Adsorption and Chemical Processing.  
50  
51 *Catalysis Today* **2006**, *115*, 2-32.
- 52  
53 3. Hunt, A. J.; Sin, E. H. K.; Marriott, R.; Clark, J. H., Generation, Capture, and Utilization of  
54  
55 Industrial Carbon Dioxide. *ChemSusChem* **2010**, *3*, 306-322.  
56  
57  
58  
59  
60

- 1  
2  
3 4. Huang, C.-H.; Phan, D. t.; Tan, C.-S., CO<sub>2</sub> Utilization. In *Handbook of Industrial Chemistry*  
4  
5 *and Biotechnology*, Kent, J. A.; Bommaraju, T. V.; Barnicki, S. D., Eds. Springer International  
6  
7 Publishing: Cham, 2017; pp 1781-1802.  
8
- 9  
10 5. Alper, E.; Orhan, O. Y., CO<sub>2</sub> Utilization: Developments in Conversion Processes. *Petroleum*  
11  
12 **2017**, 3, 109-126.  
13
- 14 6. Li, L.; Zhao, N.; Wei, W.; Sun, Y., A Review of Research Progress on CO<sub>2</sub> Capture, Storage,  
15  
16 and Utilization in Chinese Academy of Sciences. *Fuel* **2013**, 108, 112-130.  
17
- 18 7. Yu, K. M. K.; Curcic, I.; Gabriel, J.; Tsang, S. C. E., Recent Advances in CO<sub>2</sub> Capture and  
19  
20 Utilization. *ChemSusChem* **2008**, 1, 893-899.  
21
- 22 8. Rubin, E. S.; Davison, J. E.; Herzog, H. J., The Cost of CO<sub>2</sub> Capture and Storage. *International*  
23  
24 *Journal of Greenhouse Gas Control* **2015**, 40, 378-400.  
25
- 26 9. Leung, D. Y. C.; Caramanna, G.; Maroto-Valer, M. M., An Overview of Current Status of  
27  
28 Carbon Dioxide Capture and Storage Technologies. *Renewable and Sustainable Energy Reviews* **2014**,  
29  
30 39, 426-443.  
31
- 32 10. Vitillo, J. G.; Smit, B.; Gagliardi, L., Introduction: Carbon Capture and Separation. *Chemical*  
33  
34 *Reviews* **2017**, 117, 9521-9523.  
35
- 36 11. Figueroa, J. D.; Fout, T.; Plasynski, S.; McIlvried, H.; Srivastava, R. D., Advances in CO<sub>2</sub>  
37  
38 Capture Technology—the U.S. Department of Energy's Carbon Sequestration Program. *International*  
39  
40 *Journal of Greenhouse Gas Control* **2008**, 2, 9-20.  
41
- 42 12. Kanniche, M.; Gros-Bonnivard, R.; Jaud, P.; Valle-Marcos, J.; Amann, J.-M.; Bouallou, C.,  
43  
44 Pre-Combustion, Post-Combustion and Oxy-Combustion in Thermal Power Plant for CO<sub>2</sub> Capture.  
45  
46 *Applied Thermal Engineering* **2010**, 30, 53-62.  
47
- 48 13. Wang, M.; Lawal, A.; Stephenson, P.; Sidders, J.; Ramshaw, C., Post-Combustion CO<sub>2</sub> Capture  
49  
50 with Chemical Absorption: A State-of-the-Art Review. *Chemical Engineering Research and Design*  
51  
52 **2011**, 89, 1609-1624.  
53  
54  
55  
56  
57  
58  
59  
60

- 1  
2  
3 14. Mondal, M. K.; Balsora, H. K.; Varshney, P., Progress and Trends in CO<sub>2</sub> Capture/Separation  
4 Technologies: A Review. *Energy* **2012**, *46*, 431-441.  
5  
6  
7  
8 15. Olajire, A. A., CO<sub>2</sub> Capture and Separation Technologies for End-of-Pipe Applications – a  
9 Review. *Energy* **2010**, *35*, 2610-2628.  
10  
11  
12 16. Spigarelli, B. P.; Kawatra, S. K., Opportunities and Challenges in Carbon Dioxide Capture.  
13 *Journal of CO<sub>2</sub> Utilization* **2013**, *1*, 69-87.  
14  
15  
16  
17 17. Kadoura, A.; Narayanan Nair, A. K.; Sun, S., Molecular Simulation Study of Montmorillonite  
18 in Contact with Variably Wet Supercritical Carbon Dioxide. *The Journal of Physical Chemistry C*  
19 **2017**, *121*, 6199-6208.  
20  
21  
22  
23  
24 18. Romanov, V.; Soong, Y.; Carney, C.; Rush, G. E.; Nielsen, B.; O'Connor, W., Mineralization  
25 of Carbon Dioxide: A Literature Review. *ChemBioEng Review* **2015**, *2*, 231-256.  
26  
27  
28  
29 19. Klemm, O., Schemenauer, R. S., Lummerich, A., Cereceda, P., Marzol, V., Corell, D.,  
30 van Heerden, J., Reinhard, D., Gherezghiher, T., Olivier, J., et al., Fog as a Fresh-Water Resource:  
31 Overview and Perspectives. *Ambio* **2012**, *41*, 221-234.  
32  
33  
34  
35 20. Fessehaye, M.; Abdul-Wahab, S. A.; Savage, M. J.; Kohler, T.; Gherezghiher, T.; Hurni, H.,  
36 Fog-Water Collection for Community Use. *Renewable & Sustainable Energy Reviews* **2014**, *29*, 52-  
37 62.  
38  
39  
40  
41  
42 21. Domen, J. K.; Stringfellow, W. T.; Camarillo, M. K.; Gulati, S., Fog Water as an Alternative  
43 and Sustainable Water Resource. *Clean Technologies and Environmental Policy* **2014**, *16*, 235-249.  
44  
45  
46  
47 22. Khalil, B.; Adamowski, J.; Shabbir, A.; Jang, C.; Rojas, M.; Reilly, K.; Ozga-Zielinski, B., A  
48 Review: Dew Water Collection from Radiative Passive Collectors to Recent Developments of Active  
49 Collectors. *Sustainable Water Resources Management* **2016**, *2*, 71-86.  
50  
51  
52  
53 23. Snustad, I.; Røe, I. T.; Brunsvold, A.; Ervik, Å.; He, J.; Zhang, Z., A Review on Wetting and  
54 Water Condensation - Perspectives for CO<sub>2</sub> condensation. *Advances in Colloid and Interface Science*  
55 **2018**, *256*, 291-304.  
56  
57  
58  
59  
60



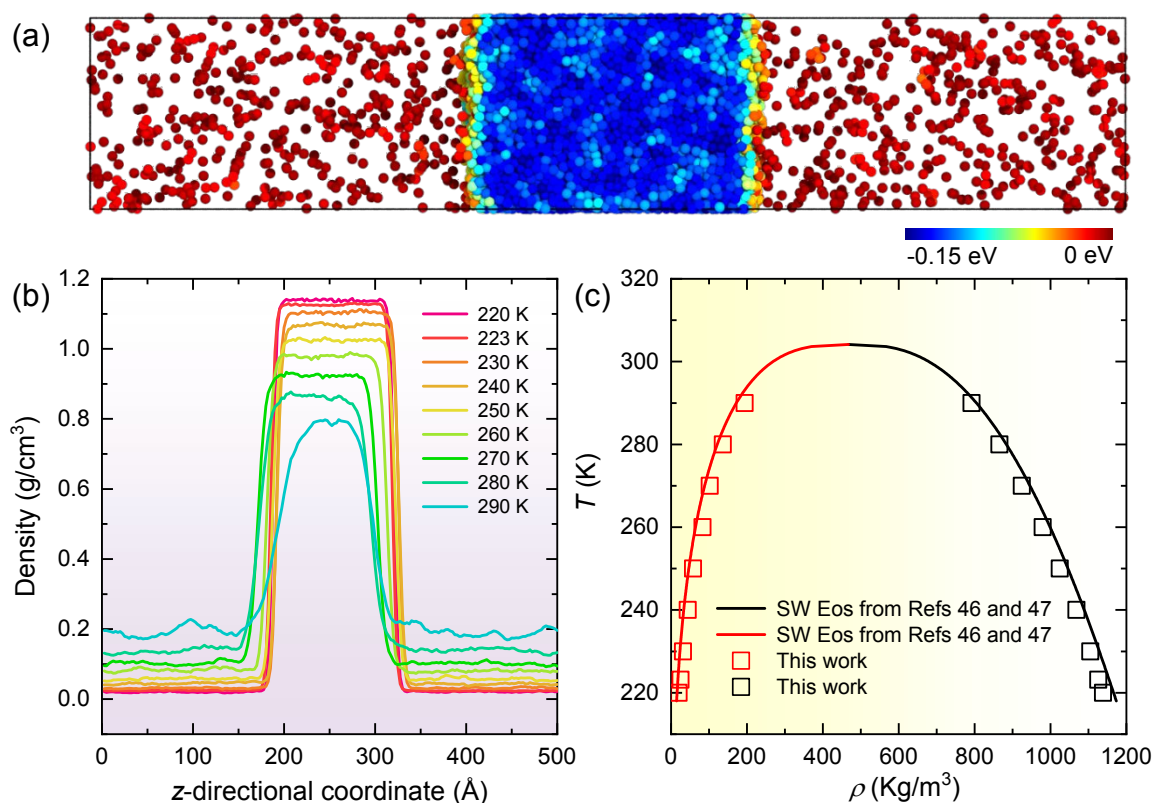
- 1  
2  
3 24. Schaef, H. T.; Glezakou, V. A.; Owen, A. T.; Ramprasad, S.; Martin, P. F.; McGrail, B. P.,  
4  
5 Surface Condensation of CO<sub>2</sub> onto Kaolinite. *Environmental Science & Technology Letters* **2014**, *1*,  
6  
7 142-145.  
8  
9  
10 25. Chen, C.; Wan, J.; Li, W.; Song, Y., Water Contact Angles on Quartz Surfaces under  
11  
12 Supercritical CO<sub>2</sub> Sequestration Conditions: Experimental and Molecular Dynamics Simulation  
13  
14 Studies. *International Journal of Greenhouse Gas Control* **2015**, *42*, 655-665.  
15  
16  
17 26. Chen, C.; Chai, Z.; Shen, W.; Li, W.; Song, Y., Wettability of Supercritical CO<sub>2</sub>-Brine-  
18  
19 Mineral: The Effects of Ion Type and Salinity. *Energy & Fuels* **2017**, *31*, 7317-7324.  
20  
21  
22 27. Liang, Y.; Tsuji, S.; Jia, J.; Tsuji, T.; Matsuoka, T., Modeling CO<sub>2</sub>-Water-Mineral Wettability  
23  
24 and Mineralization for Carbon Geosequestration. *Accounts of Chemical Research* **2017**, *50*, 1530-1540.  
25  
26  
27 28. Chen, C.; Dong, B.; Zhang, N.; Li, W.; Song, Y., Pressure and Temperature Dependence of  
28  
29 Contact Angles for CO<sub>2</sub>/Water/Silica Systems Predicted by Molecular Dynamics Simulations. *Energy*  
30  
31 *& Fuels* **2016**, *30*, 5027-5034.  
32  
33  
34 29. Chen, C.; Zhang, N.; Li, W.; Song, Y., Water Contact Angle Dependence with Hydroxyl  
35  
36 Functional Groups on Silica Surfaces under CO<sub>2</sub> Sequestration Conditions. *Environmental Science &*  
37  
38 *Technology* **2015**, *49*, 14680-14687.  
39  
40  
41 30. Javanbakht, G.; Sedghi, M.; Welch, W.; Goual, L., Molecular Dynamics Simulations of  
42  
43 CO<sub>2</sub>/Water/Quartz Interfacial Properties: Impact of CO<sub>2</sub> Dissolution in Water. *Langmuir* **2015**, *31*,  
44  
45 5812-5819.  
46  
47  
48 31. Iglauer, S.; Mathew, M. S.; Bresme, F., Molecular Dynamics Computations of Brine- CO<sub>2</sub>  
49  
50 Interfacial Tensions and Brine-CO<sub>2</sub>-Quartz Contact Angles and Their Effects on Structural and  
51  
52 Residual Trapping Mechanisms in Carbon Geo-Sequestration. *Journal of Colloid and Interface*  
53  
54 *Science* **2012**, *386*, 405-414.  
55  
56  
57 32. Jung, J.-W.; Wan, J., Supercritical CO<sub>2</sub> and Ionic Strength Effects on Wettability of Silica  
58  
59 Surfaces: Equilibrium Contact Angle Measurements. *Energy & Fuels* **2012**, *26*, 6053-6059.  
60

- 1  
2  
3 33. Liu, S.; Yang, X.; Qin, Y., Molecular Dynamics Simulation of Wetting Behavior at  
4 CO<sub>2</sub>/Water/Solid Interfaces. *Chinese Science Bulletin* **2010**, *55*, 2252-2257.  
5  
6  
7 34. Niu, D.; Tang, G. H., The Effect of Surface Wettability on Water Vapor Condensation in  
8 Nanoscale. *Scientific Reports* **2016**, *6*, 19192.  
9  
10  
11 35. Gao, S.; Liao, Q.; Liu, W.; Liu, Z., Effects of Solid Fraction on Droplet Wetting and Vapor  
12 Condensation: A Molecular Dynamic Simulation Study. *Langmuir* **2017**, *33*, 12379-12388.  
13  
14  
15 36. Ou, X.; Wang, X.; Lin, Z.; Li, J., Heterogeneous Condensation of Water on the Mica (001)  
16 Surface: A Molecular Dynamics Simulation Work. *The Journal of Physical Chemistry C* **2017**, *121*,  
17 6813-6819.  
18  
19  
20 37. Hong, S. D.; Ha, M. Y.; Balachandar, S., Static and Dynamic Contact Angles of Water Droplet  
21 on a Solid Surface Using Molecular Dynamics Simulation. *Journal of Colloid and Interface Science*  
22 **2009**, *339*, 187-195.  
23  
24  
25 38. Hirvi, J. T.; Pakkanen, T. A., Wetting of Nanogrooved Polymer Surfaces. *Langmuir* **2007**, *23*,  
26 7724-7729.  
27  
28  
29 39. Šolc, R.; Tunega, D.; Gerzabek M., H.; Woche S., K.; Bachmann, J., Wettability of Organically  
30 Coated Tridymite Surface – Molecular Dynamics Study. In *Pure and Applied Chemistry*, **2015**; Vol.  
31 87, p 405.  
32  
33  
34 40. Andrews, J. E.; Sinha, S.; Chung, P. W.; Das, S., Wetting Dynamics of a Water Nanodrop on  
35 Graphene. *Physical Chemistry Chemical Physics* **2016**, *18*, 23482-23493.  
36  
37  
38 41. W. Xu; Z. Lan; B. L. Peng; R. F. Wen; Ma, X. H., Effect of Surface Free Energies on the  
39 Heterogeneous Nucleation of Water Droplet: A Molecular Dynamics Simulation Approach. *The*  
40 *Journal of Chemical Physics* **2015**, *142*, 054701.  
41  
42  
43 42. Koishi, T.; Yasuoka, K.; Fujikawa, S.; Ebisuzaki, T.; Zeng, X. C., Coexistence and Transition  
44 between Cassie and Wenzel State on Pillared Hydrophobic Surface. *Proceedings of the National*  
45 *Academy of Sciences* **2009**, *106*, 8435-8440.  
46  
47  
48  
49  
50  
51  
52  
53  
54  
55  
56  
57  
58  
59  
60

- 1  
2  
3 43. Mishin, Y.; Mehl, M. J.; Papaconstantopoulos, D. A.; Voter, A. F.; Kress, J. D., Structural  
4 Stability and Lattice Defects in Copper: Ab Initio, Tight-Binding, and Embedded-Atom Calculations.  
5  
6 *Physical Review B* **2001**, *63*, 224106.  
7  
8  
9  
10 44. Daw, M. S.; Baskes, M. I., Embedded-Atom Method: Derivation and Application to Impurities,  
11 Surfaces, and Other Defects in Metals. *Physical Review B* **1984**, *29*, 6443-6453.  
12  
13  
14 45. Avendaño, C.; Lafitte, T.; Galindo, A.; Adjiman, C. S.; Jackson, G.; Müller, E. A., Saft- $\Gamma$  Force  
15 Field for the Simulation of Molecular Fluids. 1. A Single-Site Coarse Grained Model of Carbon  
16 Dioxide. *The Journal of Physical Chemistry B* **2011**, *115*, 11154-11169.  
17  
18  
19  
20 46. J. E. Jones; Sc., D., On the Determination of Molecular Fields. — II. From the Equation of  
21 State of a Gas. *Proceedings of the Royal Society of London. Series A* **1924**, *106*, 463-477.  
22  
23  
24  
25 47. C. A. Leng; J. S. Rowlinson; F. R. S.; Thompson, S. M., The Gas – Liquid Surface of the  
26 Penetrable Sphere Model. *Proceedings of the Royal Society of London. A. Mathematical and Physical*  
27 *Sciences* **1976**, *352*, 1-23.  
28  
29  
30  
31  
32 48. Weeks, J. D., Structure and Thermodynamics of the Liquid–Vapor Interface. *The Journal of*  
33 *Chemical Physics* **1977**, *67*, 3106-3121.  
34  
35  
36  
37 49. Wilhelmsen, Ø.; Aasen, A.; Skaugen, G.; Aursand, P.; Austegard, A.; Aursand, E.; Gjennestad,  
38 M. A.; Lund, H.; Linga, G.; Hammer, M., Thermodynamic Modeling with Equations of State: Present  
39 Challenges with Established Methods. *Industrial & Engineering Chemistry Research* **2017**, *56*, 3503-  
40 3515.  
41  
42  
43  
44  
45  
46 50. Roland Span; Wagner, W., A New Equation of State for Carbon Dioxide Covering the Fluid  
47 Region from the Triple-Point Temperature to 1100 K at Pressures up to 800 Mpa. *Journal of Physical*  
48 *and Chemical Reference Data* **1996**, *25*, 1509-1596.  
49  
50  
51  
52  
53 51. Müller, E. A.; Jackson, G., Force-Field Parameters from the Saft- $\gamma$  Equation of State for Use  
54 in Coarse-Grained Molecular Simulations. *Annual Review of Chemical and Biomolecular Engineering*  
55 **2014**, *5*, 405-427.  
56  
57  
58  
59  
60

- 1  
2  
3 52. Hoang, H.; Delage-Santacreu, S.; Galliero, G., Simultaneous Description of Equilibrium,  
4 Interfacial, and Transport Properties of Fluids Using a Mie Chain Coarse-Grained Force Field.  
5  
6  
7  
8 *Industrial & Engineering Chemistry Research* **2017**, *56*, 9213-9226.  
9  
10  
11  
12  
13  
14  
15  
16  
17  
18  
19  
20  
21  
22  
23  
24  
25  
26  
27  
28  
29  
30  
31  
32  
33  
34  
35  
36  
37  
38  
39  
40  
41  
42  
43  
44  
45  
46  
47  
48  
49  
50  
51  
52  
53  
54  
55  
56  
57  
58  
59  
60

1  
2  
3 **Figures and Captions**  
4  
5  
6



33 Figure 1 CO<sub>2</sub> vapor-liquid system. (a) A representative side-viewd snapshot of vapor-liquid  
34 coexistence of CO<sub>2</sub> in a box with dimensions of 92 × 92 × 500 Å<sup>3</sup>. Molecular coarse-grained (CG)  
35 beads are colored on the basis of their potential energies for enhanced visibility. (b) Density profiles  
36 of the vapor-liquid equilibrium at temperatures varying from 220 K to 290 K. (c) Comparison of  
37 temperature-density of vapor-liquid coexistence of CO<sub>2</sub> with equilibrium of state (EoS) data<sup>46-47</sup>.  
38  
39  
40  
41  
42  
43  
44  
45  
46  
47  
48  
49  
50  
51  
52  
53  
54  
55  
56  
57  
58  
59  
60

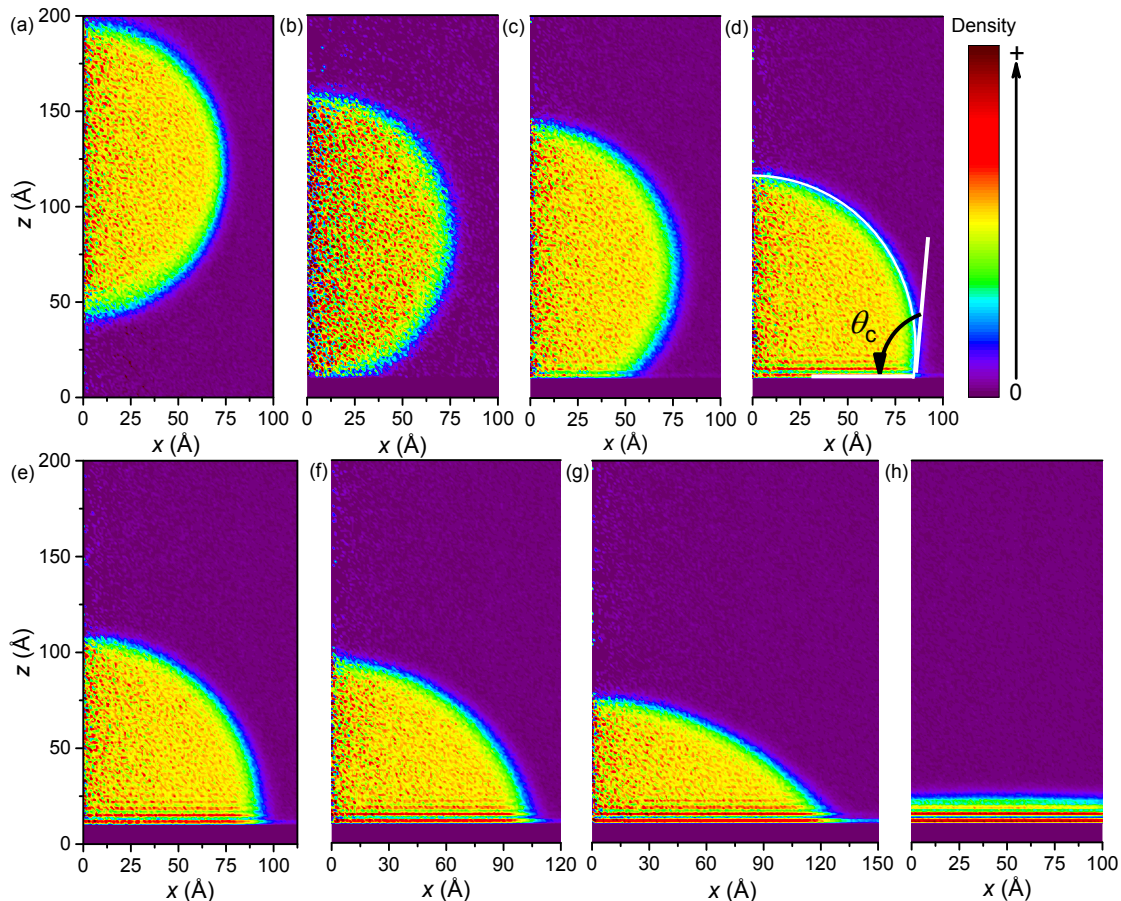


Figure 2 Relative density maps of CO<sub>2</sub> droplets on a Cu-like solid surface with a CO<sub>2</sub>-surface interaction parameter  $\epsilon_{\text{CO}_2\text{-Cu}}$  of (a) 0.001 eV, (b) 0.003 eV, (c) 0.005 eV, (d) 0.008 eV, (e) 0.009 eV, (f) 0.01 eV, (g) 0.012 eV, and (h) 0.015 eV, respectively.

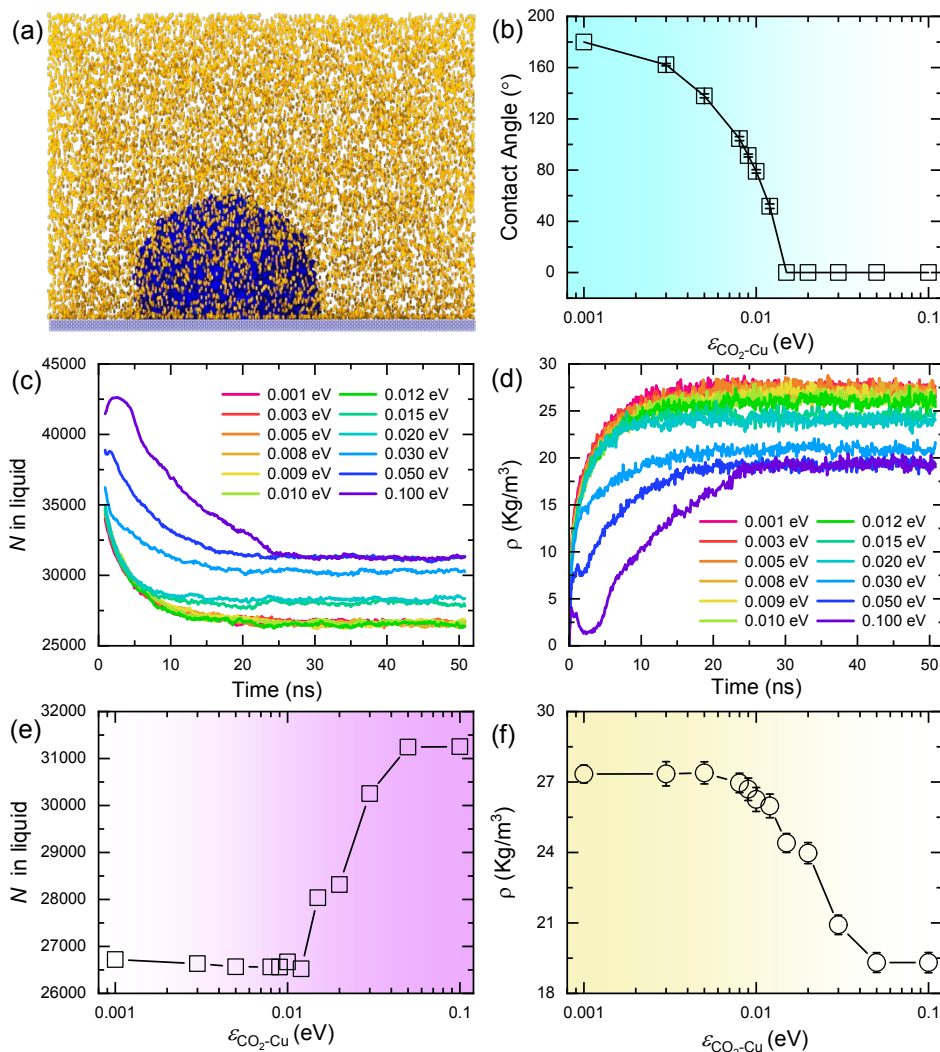


Figure 3 CO<sub>2</sub>-solid surface-system analysis. (a) A snapshot of a CO<sub>2</sub> droplet and vapor contacting with Cu-like surface having an energy interaction parameter of  $\epsilon_{\text{CO}_2\text{-Cu}} = 0.008$  eV in equilibrium. Vaporized and liquid CO<sub>2</sub> molecules are yellow- and blue-highlighted for clarification, respectively. (b) Contact angle of CO<sub>2</sub> droplet as a function of interaction energy  $\epsilon_{\text{CO}_2\text{-Cu}}$ . (c) and (d) Variation in number of liquid-state CO<sub>2</sub> and the density of the gas phase with the MD simulation time, respectively. (e) and (f) Variation in number of liquid-state CO<sub>2</sub> and the density of the gas phase with  $\epsilon_{\text{CO}_2\text{-Cu}}$ , respectively.

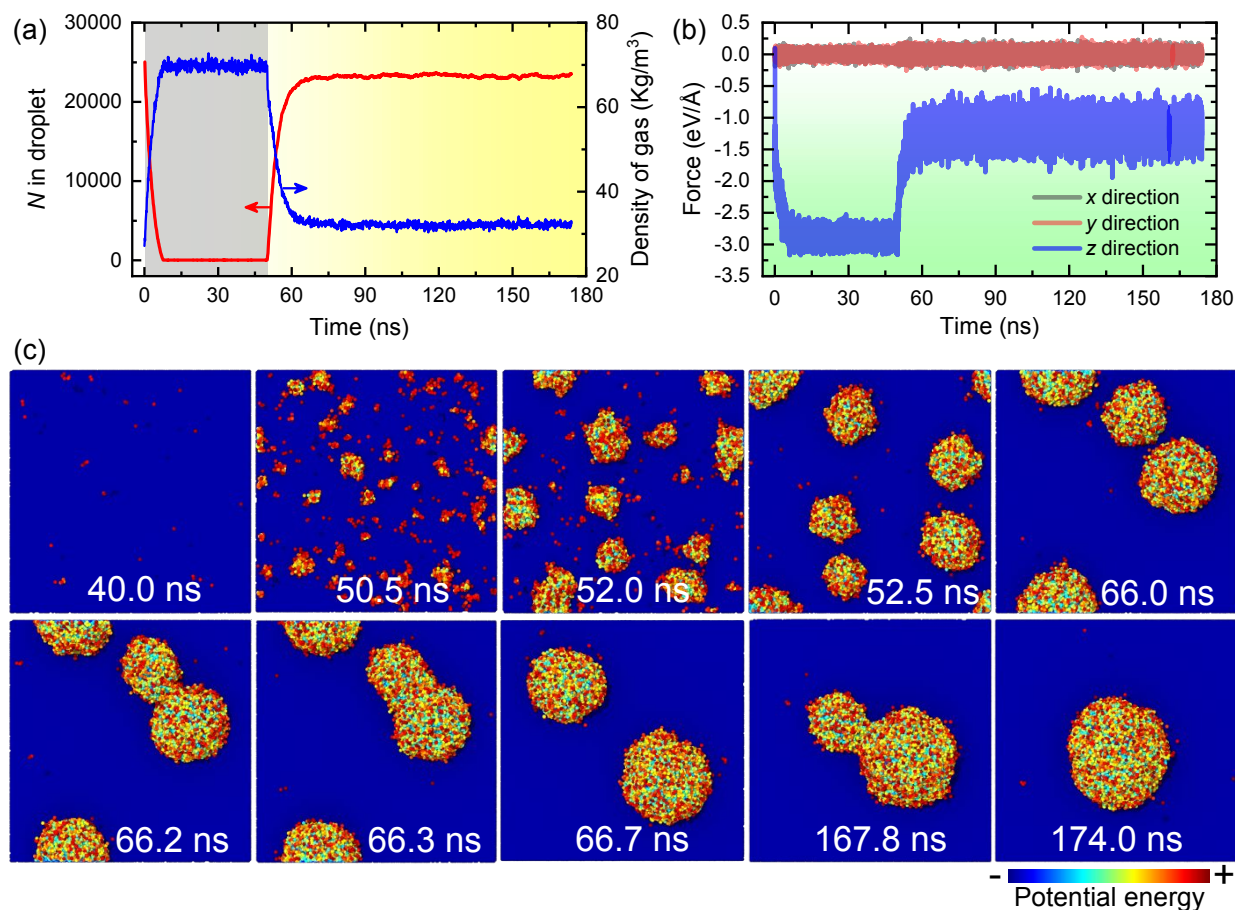


Figure 4 Analysis of vaporization and condensation of a CO<sub>2</sub> droplet on a Cu-like solid surface with an interaction  $\varepsilon_{\text{CO}_2\text{-Cu}} = 0.008$  eV. (a) Number of CO<sub>2</sub> molecules in the droplet and the density of CO<sub>2</sub> gas phase as a function of MD simulation time. (b) Total interaction forces between CO<sub>2</sub> and Cu-like solid surface against MD simulation time along the three orthogonal directions. (c) Snapshots of the condensation process of CO<sub>2</sub> droplet on a cooling Cu-like solid surface. CG beads in the condensed droplet are colored according to their potential energies. CG gas beads that have potential energies  $> -0.05$  eV are removed for enhanced visibility.



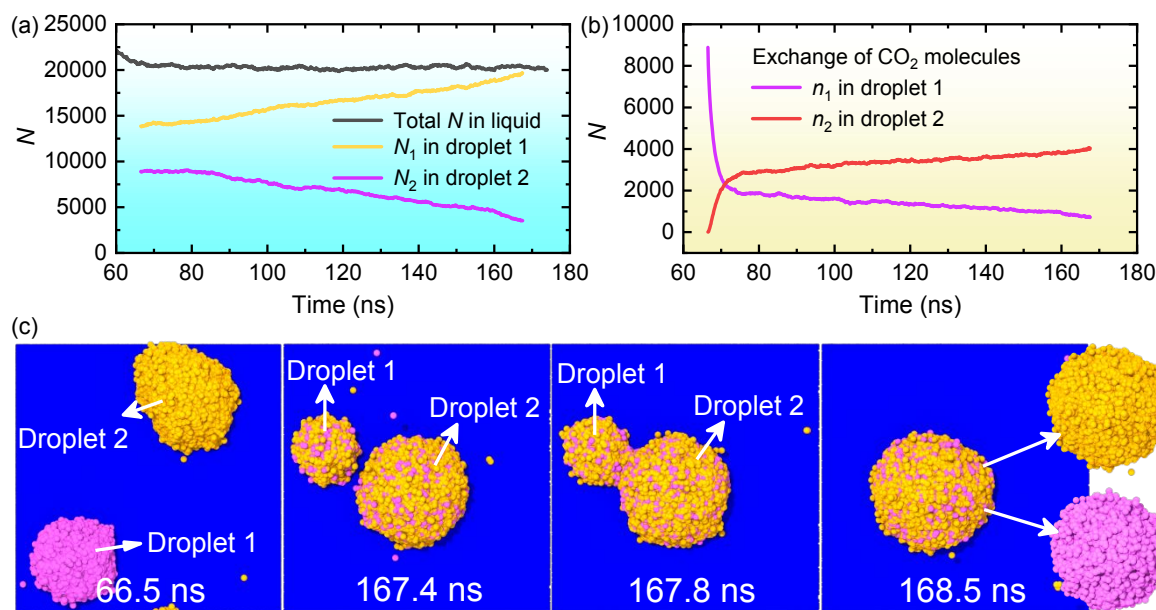


Figure 5 Condensation characteristics of a CO<sub>2</sub> droplet on a Cu-like solid surface. (a) Variations in number ( $N_1$ ,  $N_2$ ) of CO<sub>2</sub> molecules of two droplets and their total number ( $N$ ) of CO<sub>2</sub> molecules with MD condensation time. (b) Exchange of CO<sub>2</sub> molecules between two droplets during the condensation process. (c) A sequence of snapshots illustrating the molecular exchange between two condensed droplets and Ostwald ripening and coalescence of two condensed CO<sub>2</sub> droplets during the condensation process. Coarse-grained (CG) beads of CO<sub>2</sub> in gas state are removed for clarification. For enhanced visualization of the exchange of CO<sub>2</sub> molecules, the two condensed CO<sub>2</sub> droplets on the Cu-like surface are purple- and yellow-highlighted, respectively. At the condensation time 168.5 ns, a droplet formed by coalescence of two droplets is composed of purple- and yellow-colored CO<sub>2</sub> molecules, explaining the molecular exchange during the condensation process. Particularly, purple- and yellow-colored CO<sub>2</sub> molecules (indicated by the arrows) are taken out from the formed droplet for showing the homogeneous distribution.

## TOC graphic

